

CINNAMON: A hybrid approach to change point detection and parameter estimation in single-particle tracking data

Jakub Malinowski^{1,3}, Marcin Kostrzewska², Michał Balcerek¹,
Weronika Tomczuk¹, Janusz Szwabiński¹

¹ Hugo Steinhaus Center, Faculty of Pure and Applied Mathematics, Wrocław University of Science and Technology, Wybrzeże Stanisława Wyspiańskiego 27, 50-370 Wrocław, Poland

² Department of Artificial Intelligence, Faculty of Information and Communication Technology, Wrocław University of Science and Technology, Wybrzeże Stanisława Wyspiańskiego 27, 50-370 Wrocław, Poland

³Dioscuri Centre in Topological Data Analysis, Mathematical Institute, Polish Academy of Sciences, ul. Śniadeckich 8, 00-656 Warsaw, Poland

E-mail: jakub.malinowski@pwr.edu.pl

Abstract.

Change point detection has become an important part of the analysis of the single-particle tracking data, as it allows one to identify moments, in which the motion patterns of observed particles undergo significant changes. The segmentation of diffusive trajectories based on those moments may provide insight into various phenomena in soft condensed matter and biological physics. In this paper, we propose CINNAMON, a hybrid approach to classifying single-particle tracking trajectories, detecting change points within them, and estimating diffusion parameters in the segments between the change points. Our method is based on a combination of neural networks, feature-based machine learning, and statistical techniques. It has been benchmarked in the second Anomalous Diffusion Challenge. The method offers a high level of interpretability due to its analytical and feature-based components. A potential use of features from topological data analysis is also discussed.

1. Introduction

Single-particle tracking (SPT) is a class of experimental techniques and mathematical algorithms that allow small particles to be followed with nanoscale spatial localization and millisecond temporal resolution [1]. It has been introduced by Perrin [2] and Nordlund [3], evolved in the last century, and became a popular tool that allowed quantitative analysis of particles moving inside living cells [4]. For example, SPT experiments can directly observe the diffusion of lipids and proteins in cell membranes, providing significant insight into their structure.

In a typical SPT experiment, the molecule of interest is labeled with an observable tag. The positions of the latter are tracked over a number of time steps, and then linked into a time series called trajectory. Possible tags include gold nanoparticles [5], quantum dots [6], fluorophores [7] or latex beads [8]. The trajectories are then analyzed to infer, among other things, the underlying model governing the motion of particles.

Molecules with the same chemical identity can display different motion patterns as a result of interactions with the complex environment where the diffusion takes place. Potential mechanisms that impact their behavior include lipid microdomains [9, 10], compartmentalization by the cytoskeleton [6, 11], protein-protein interactions [8] and inhomogeneity in the plasma membrane environment [12].

A number of methods has been already proposed for analyzing SPT data. The most common approach is based on the mean-squared displacement (MSD), which measures the deviation of particles with respect to a reference position [13, 14]. An MSD linear in time corresponds to Brownian motion (a.k.a. normal diffusion), which describes the movement of a microscopical particle as a consequence of thermal forces. Any deviations from that linear behavior are called anomalous diffusion [15].

Although quite simple, the MSD-based analysis of trajectories is challenging because the trajectories are usually short and noisy. Consequently, several other approaches have been introduced as well. For example, the radius of gyration [16], the velocity autocorrelation function [17, 18], the time-dependent directional persistence of trajectories [19], the distribution of directional changes [20], the mean maximum excursion method [21], or the fractionally integrated moving average framework [22] may efficiently replace the MSD estimator for analysis purposes.

Due to the advent of powerful GPUs and TPUs and the recent advances in machine learning (ML) algorithms, the latter has become an interesting alternative for the analysis of anomalous diffusion. ML is already known to excel in different domains including computer vision [23], speech recognition [24] and natural language processing [25]. Its first applications to SPT data turned out to be promising, even though the characterization of particle motion remains very challenging [26–39].

To gain some insight into the performance of various methods, a group of researchers has launched the Anomalous Diffusion (AnDi) Challenge in 2021 [40]. The goal of the competition was actually threefold. In addition to benchmarking existing approaches on standardized data sets, the organizers also aimed to stimulate the development of new methods and to gain new insights into anomalous diffusion. The challenge was divided into three tasks: (1) inferring the anomalous diffusion exponent from single trajectories, (2) classification of diffusion models, and (3) segmentation of trajectories. The results of the challenge clearly showed that deep learning methods based on deep neural networks significantly outperform the other ones (including feature-based machine learning), with statistical approaches being the worst [40].

The discussion between members of various research communities sparked by the AnDi Challenge emphasized the need for a deeper understanding of biologically relevant phenomena present in SPT data. In particular, the detection of switches between

different diffusive behaviors within a single trajectory requires further elaboration. These switches serve as valuable indicators for the occurrence of interactions within the system. For example, molecules may exhibit variations in diffusion coefficients due to processes like dimerization [41], ligand binding [42] or conformational changes [43]. And shifts in their mode of motion may be attributed to transient immobilization or confinement at specific scaffolding sites [11, 41, 44, 45].

In response to this demand, the 2nd AnDi Challenge has been designed and launched in 2023 [46]. Its focus was on revealing heterogeneity rather than anomalous diffusion, but, of course, the latter was also present in the provided datasets. Similarly to the first edition of the challenge, the organizers aimed to benchmark existing methods for trajectory segmentation [47–50]. Moreover, the development of new methods should be encouraged in order to detect subtle changes in diffusion properties in systems where they have been overlooked so far.

In this paper, we are going to present our contribution to the 2nd AnDi Challenge. CINNAMON (i.e. Change poInt detectioN aNd pArameter estiMation fOr aNomalous diffusion) is a hybrid method using a combination of neural networks, feature-based algorithms, and analytical methods. In the single-trajectory task within the competition, it first identifies the change points by making use of a neural network consisting of a DAIN layer for data standardization, several 1D convolutional layers, LSTM layers and an attention layer [51]. Then, in each segment, the anomalous exponent is estimated with a gradient boosting method based on the features designed for the first AnDi Challenge [52]. For the diffusion coefficient, an estimator from [53] is used. In the ensemble task, another neural network is applied to identify the model which is used to generate trajectories. Its architecture is very similar to that for change point detection, as it contains the same building blocks.

The paper is structured as follows. In Sec. 2, the competition setup of the 2nd AnDi Challenge is briefly summarized. Then, in Sec. 3, our contribution to the challenge is presented. Results are shown and discussed in Sec. 4. Some concluding remarks may be found in Sec. 5. And finally, Appendix A contains a few technical details of our method.

2. Competition setup

The details of the 2nd AnDi Challenge may be found in Ref. [46]. In this section we briefly summarize them for the convenience of a reader.

2.1. Datasets and ground truth

For the datasets used in the challenge, we relied on the `andi-datasets` Python package [40] provided by the authors of the competition. It allows the generation of synthetic data representing a variety of diffusive behaviours. All the simulations are based on fractional Brownian motion (FBM), a mathematical model that accounts for both normal and anomalous diffusion [54]. FBM is a zero-mean Gaussian process $(B_H(t))_{t \geq 0}$

characterized by the autocovariance function

$$\langle B_H(t)B_H(s) \rangle = \frac{K}{2} (t^{2H} + s^{2H} - |t - s|^{2H}), \quad (1)$$

for any time $t, s \geq 0$ and the generalized diffusion coefficient $K > 0$ with units $[K] = \frac{\text{length}^2}{\text{time}^{2H}}$. The parameter $H \in (0, 1)$, often referred to as the Hurst exponent, directly relates to the anomalous diffusion exponent α through the equation $\alpha = 2H$. When $H = \frac{1}{2}$, the process corresponds to standard Brownian motion, with independent increments and a linear mean-squared displacement. For $H < \frac{1}{2}$, the process exhibits subdiffusion, often related to crowded environments. It corresponds to a slower than linear MSD growth. In contrast, for $H > \frac{1}{2}$, FBM is super-diffusive, which implies that motion is persistent and MSD grows faster than a linear function.

The generalizations of FBM considered in the challenge are based on physical models of motion and interactions. Among them, there are:

- Single-state model (SSM) where the particles diffuse according to a single diffusion state. SSM serves as a baseline case, where no transitions between different motion states occur. It is often used as a control to assess false positives in methods that detect changes in the diffusive behavior. Biologically, this model can represent molecules such as lipids in the plasma membrane that diffuse freely without undergoing significant interactions or state changes.
- Multi-state model (MSM) where particles diffuse according to a time-dependent multi-state model of diffusion with transient changes of K and/or α . MSM describes particles that transition between different diffusion states over time. These transitions involve changes in the generalized diffusion coefficient K , the anomalous diffusion exponent α , or both. The switches between states can be spontaneous or induced by interactions with the environment, leading to a heterogeneous motion pattern. In a biological context, MSM can model proteins that alter their mobility due to conformational changes, binding to ligands, or interactions with cellular structures. The duration spent in each state and the frequency of transitions determine the complexity of the resulting trajectory.
- Dimerization model (DIM) where the particles diffuse according to a 2-state model of diffusion, with transient changes of K and/or α due to encounters with other diffusing particles. In this model, a particle moves freely until it interacts with another diffusing particle. Upon encountering its binding partner, the two particles form a temporary complex (dimer), which alters their diffusion properties. This change can manifest as a shift in the diffusion coefficient or the anomalous diffusion exponent, reflecting the fact that the dimer is typically larger and may experience different interactions with the surrounding environment. Once the binding interaction ends, the two particles separate and resume their original diffusive behavior. DIM is particularly relevant in a biological context where molecular interactions play a crucial role, such as protein dimerization, receptor-ligand binding, or transient macromolecular assemblies.

- Transient-confinement model (TCM) where particles diffuse according to a space-dependent 2-state diffusion model. In the TCM, particles diffuse freely until they enter confined regions, where their mobility is reduced due to spatial constraints. These confined regions act like compartments with osmotic boundaries that allow entry and exit. This model represents biological scenarios where molecules experience temporary entrapment, such as proteins diffusing in the plasma membrane and being transiently confined by lipid rafts or clathrin-coated pits. The confinement in TCM is not absolute; particles can escape after some time.
- Quenched-trap model (QTM) where particles diffuse according to a space-dependent 2-state model of diffusion. QTM represents a scenario where particles undergo intermittent immobilization by binding to static structures within the environment. Instead of being in a confined zone, particles become “trapped” at specific, fixed locations where their motion is temporarily halted. This is relevant for biological cases where molecules are sequestered due to interactions with elements like the cytoskeleton or scaffolding proteins. Unlike TCM, where diffusion is still possible within the confined region, in QTM, the trapped state results in a complete stop in motion until the particle is released.

Example trajectories generated with the above models are presented in Figure 1. There are no changes in the motion pattern in the SSM (left plot). All others reveal interaction-induced switches between different diffusive regimes.

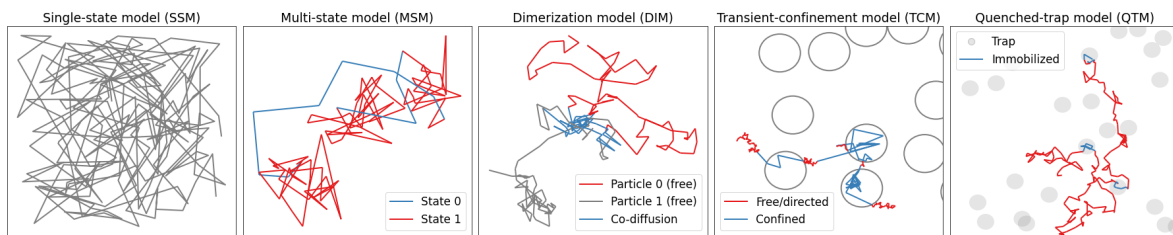


Figure 1. Physical models of motion and interactions in diffusion processes. Panels from left to right: single-state model (SSM) without changes of diffusion; multi-state model (MSM) with time-dependent changes between diffusive states (red and blue); dimerization model (DIM) with interactions between particles (red and grey) and their transient co-diffusion (blue) with a different motion; transient-confinement model (TCM) with particles diffusing inside (blue) and outside (red) compartments (circles); quenched-trap model (QTM) where a particle is transiently immobilized (blue) in specific regions (grey areas) or diffuses freely (red).

2.2. Competition design

The 2nd AnDi Challenge was designed to evaluate methods for analyzing motion changes in single-molecule experiments and was divided into two tracks. In the first one, the participants worked with raw video data, extracting motion information directly

from simulated microscopy recordings. In the second track, participants analyzed preprocessed particle trajectories, i.e., numerical values of coordinates of particles rather than images. Our team focused on the second track, dedicating our efforts to analyzing preprocessed data rather than working with raw video recordings.

In each track, participants could compete in two different tasks. The first was the ensemble task, where participants provided a statistical description of diffusion behavior across an experiment. This included identifying the underlying model, determining the number of diffusive states, and estimating the statistical properties of the diffusion coefficient K and anomalous exponent α . The second was the single-trajectory task, in which participants analyzed individual particle trajectories to detect change points marking transitions between different motion states (see Fig. 2). For each segment, they estimated the diffusion coefficient, the anomalous exponent, and classified the type of diffusion.

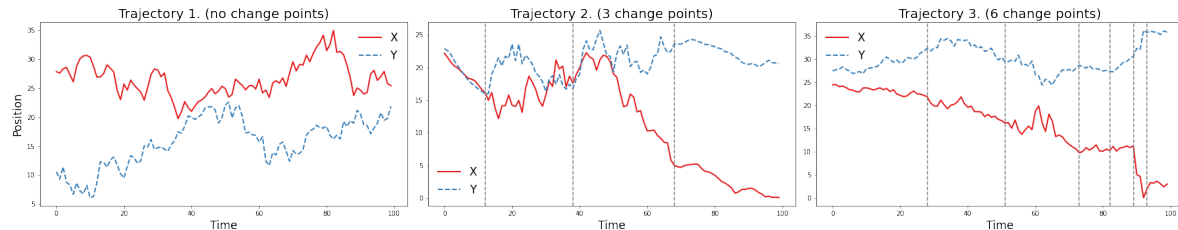


Figure 2. Exemplary particle trajectories with change points, which are indicated with dashed vertical lines. The number of change points increases from 0 (left panel), to 3 (middle panel), and 6 (right panel). Both X (solid red lines) and Y (dashed blue lines) coordinates of a trajectory follow the same underlying state.

3. Methods

The method we proposed for the first AnDi Challenge was using a set of human-engineered features and the extreme gradient boosting classifier to identify diffusion modes from single trajectories [40]. We deliberately decided to pick traditional machine learning over the state-of-the-art technology based on deep neural networks due to its superior interpretability. Indeed, our approach allowed us to identify factors crucial for the determination of a diffusion type in every data sample. Moreover, even though the performance of our original method was noticeably smaller than the top three deep learning solutions, we were able to significantly improve it with a further extension of the feature set [52].

Our contribution to the 2nd AnDi Challenge roots, at least to some extent, in our previous experiences. CINNAMON (Change poInt detectioN aNd pArameter estiMation fOr aNomalous diffusion) is a hybrid method using a combination of neural networks, feature-based algorithms, and analytical methods. Its details are presented in the remaining part of this section. The implementation of the method may be found on Github [55].

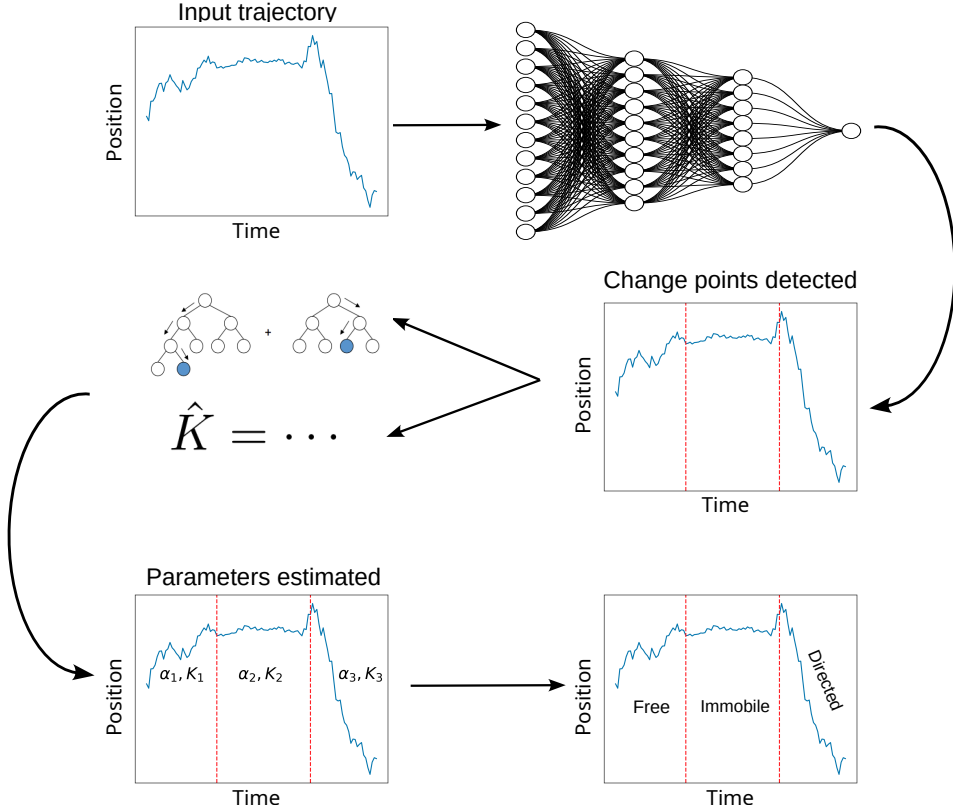


Figure 3. CINNAMON method for single-trajectory task. A neural network identifies the change points within an input trajectory. Then, in each segment, the anomalous exponent α is estimated with a gradient boosting method based on the features designed for the first AnDi Challenge [52]. For the generalized diffusion coefficient K , an estimator from [53] is used (see Sec. 3.1.3). Finally, the segments are classified based on the values of α and K .

3.1. Single-trajectory task

The scheme of our method for the single-trajectory task is presented in Fig. 3. A neural network is used to identify change points within an input trajectory. Then, in each segment, the anomalous exponent α is estimated with a gradient boosting method with the features engineered for the first AnDi challenge [40, 52]. For the generalized diffusion coefficient K , an estimator from [53] is used. Finally, the segments are classified according to the values of α and K . The details of each step of the procedure are described below.

3.1.1. Change point detection Our change point detection method builds upon the framework proposed by Li et al. [56], employing a classifier-based approach to predict change points within trajectory subsequences. The architecture begins with a Deep Adaptive Input Normalization (DAIN) layer [57], which learns optimal normalization parameters for the time series data, enhancing the model's ability to handle non-stationary sequences. The neural architecture then employs two 1D convolutional

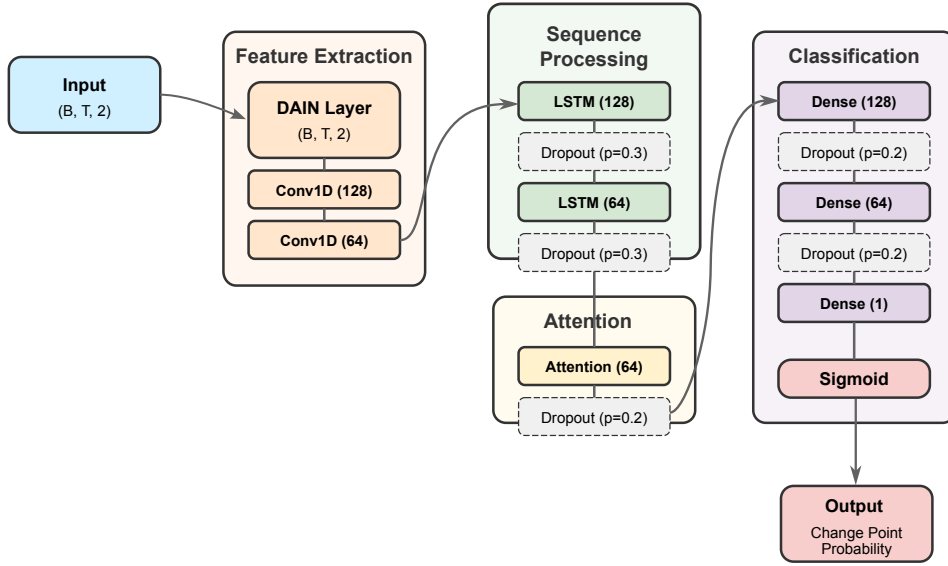


Figure 4. The architecture of neural network for change point detection. B and T on the diagram represent batch size and length of the sequence, respectively. p is the dropout rate. The architecture begins with a Deep Adaptive Input Normalization (DAIN) layer, which learns optimal normalization parameters for the time series data. The neural architecture then employs two 1D convolutional layers, respectively, followed by two LSTM layers and an attention layer with 64 units. The final prediction is made through three dense layers of decreasing size (128, 64, 1 neurons), with dropout layers [61] included to prevent overfitting. The first two dropout layers after the LSTM layers have the probability p (i.e., the dropout rate) set to 0.3, while the subsequent dropout layers have $p = 0.2$. The complete architecture with output shapes for each layer is presented in Fig. 4. ReLU activation functions are used throughout the network, except for the final layer which is followed by a sigmoid activation to output probabilities.

layers [58] with 128 and 64 feature maps, respectively, followed by two LSTM layers [59] containing 128 and 64 cells, and an attention layer [60] with 64 units. The final prediction is made through three dense layers of decreasing size (128, 64, 1 neurons), with dropout layers [61] included to prevent overfitting. The first two dropout layers after the LSTM layers have the probability p (i.e., the dropout rate) set to 0.3, while the subsequent dropout layers have $p = 0.2$. The complete architecture with output shapes for each layer is presented in Fig. 4. ReLU activation functions are used throughout the network, except for the final layer which is followed by a sigmoid activation to output probabilities. The model is trained using binary cross-entropy loss.

The weights and biases of the neural network were initialized with the popular Glorot method [62]. The model was trained over 10 epochs using the Adam optimizer [63] with a learning rate equal to 0.001 and a batch size of 32. Training and validation metrics demonstrated consistent performance improvement with no signs of overfitting.

For a trajectory $X = (x_1, \dots, x_t)$, the trained classifier $\varphi : \mathbb{R}^{d \times T} \rightarrow [0, 1]$ analyzes sliding windows of length T , generating probabilities $p_i = \varphi(X[i, i+T])$, which indicate the likelihood of a change point occurring (see Fig. 5). The detection algorithm identifies segments where p_i exceeds a threshold γ ($\gamma = 0.95$ was used throughout this work). Within each segment, the precise location of the change point is determined by finding

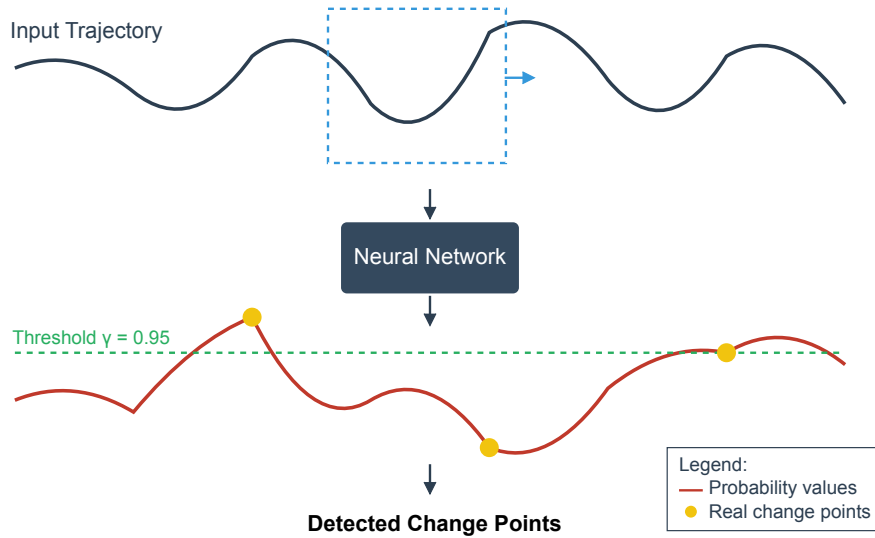


Figure 5. Explanation of the change point detection method. The classifier shown in Fig. 4 analyses a window of length $T = 15$ sliding over a trajectory in order to generate probabilities p_i , which indicate the likelihood of a change point occurring. The algorithm identifies then segments where p_i exceeds a threshold $\gamma = 0.95$. Within each segment, the precise location of the change point is determined by finding the position where the probability reaches its maximum value. In the example presented in the diagram, the left change point would be identified correctly, the right one would be found as well but at wrong position and the method would fail to identify the point in the middle.

the position where the probability reaches its maximum value. This approach eliminates the issue of detecting consecutive change points, as only a single point from each continuous segment above the threshold is classified as a change point. The method assumes that change points can be detected through local patterns in the trajectory data, with the window length T determining the scale of these patterns. Experiments revealed that while classifiers trained on longer subsequences ($T = 20$) showed better classification accuracy, a window length of $T = 15$ provides the optimal balance between detection accuracy and the ability to identify closely spaced change points.

3.1.2. Estimation of α Building on our experience from the 1st AnDi Challenge [52], we decided to use the gradient boosting method [64] together with the feature set described in Appendix A to estimate the anomalous exponent α .

Gradient boosting is an ensemble learning method that builds a strong predictive model by sequentially training weak learners, typically decision trees [65]. At each iteration, a new tree is fitted to correct the errors made by the previous trees, using the gradient of the loss function as a guide (see Fig. 6 for an illustration of the training process). This stepwise improvement minimizes prediction errors while maintaining flexibility in handling complex data distributions. Compared to other ensemble methods

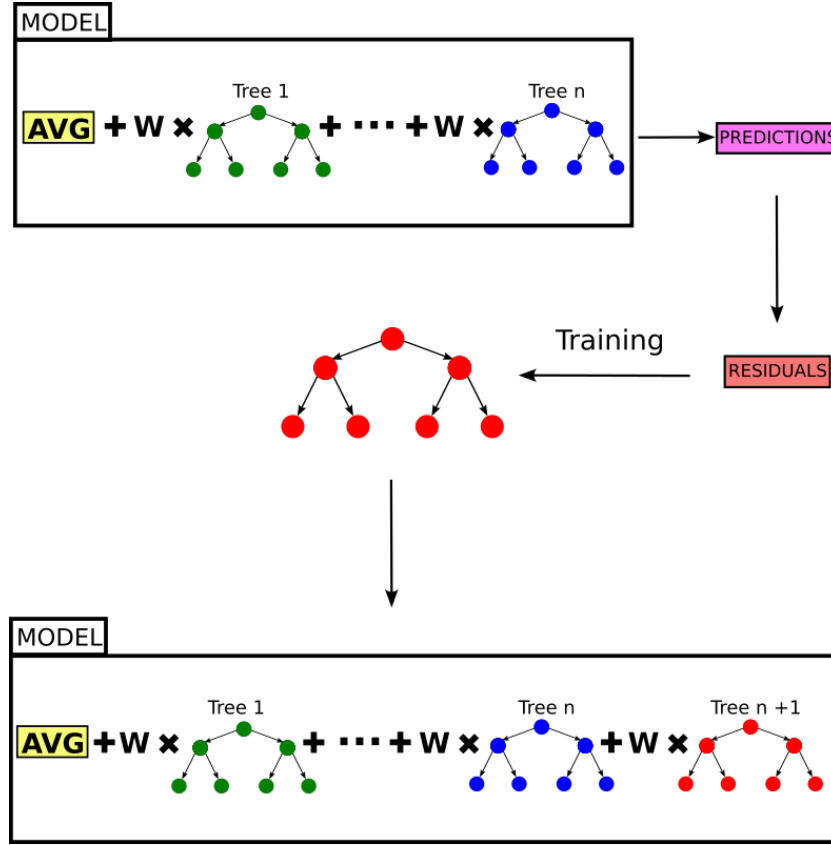


Figure 6. Construction process of the gradient boosting regressor. The algorithm begins with a naive model that simply returns the mean of training labels (called AVG in the plot). It then progressively improves prediction accuracy by sequentially adding new decision trees, each trained specifically on the errors (residuals) generated by the combined ensemble of previous trees. This iterative approach of making many small corrections to address remaining errors leads to better generalization performance and robustness compared to single decision trees. Each new tree focuses on the samples that were most challenging for the existing ensemble. The symbol W in the model stands for the learning rate hyperparameter.

like random forest, gradient boosting tends to achieve higher predictive accuracy but may require careful tuning to avoid overfitting [66].

3.1.3. Estimation of K Estimating the anomalous diffusion coefficient K usually requires a careful approach [53]. Even if the experimental data exhibits a behaviour adequate to some theoretical model of anomalous diffusion, it is always disturbed by some measurement noise

$$\tilde{X}(t) = X(t) + \xi(t), \quad (2)$$

where $X(t)$ is a pure anomalous diffusion process with diffusion coefficient K and exponent α , $\xi(t)$ denotes noise, which is assumed to be independent of $X(t)$ and normally distributed with zero mean and variance σ^2 for each t .

The ensemble-average MSD for such a model is given by

$$\langle \tilde{X}^2(n\Delta t) \rangle = 2K(n\Delta t)^\alpha + \sigma^2, \quad (3)$$

which is significantly different from the pure anomalous diffusion model for which $\sigma^2 = 0$.

The last expression may be rewritten as

$$\langle \tilde{X}^2(n\Delta t) \rangle = 2K(n\Delta t)^\alpha + \sigma^2 = 2K(n\Delta t)^\alpha \left(1 + \frac{\sigma^2}{2K(n\Delta t)^\alpha} \right) \quad (4)$$

Taking the logarithms of both sides yields

$$\ln \langle \tilde{X}^2(n\Delta t) \rangle = \ln(2K) + \alpha \ln(n\Delta t) + \ln \left(1 + \frac{\sigma^2}{2K(n\Delta t)^\alpha} \right). \quad (5)$$

For sufficiently large values of $n\Delta t$, the noise term disappears, leading to a linear dependence:

$$\ln \langle \tilde{X}^2(n\Delta t) \rangle \approx \ln(2K) + \alpha \ln(n\Delta t). \quad (6)$$

Following the classical approach (Approach I in Ref. [53]), the estimation of K and α is performed through a least-squares fitting. The anomalous diffusion exponent α is then estimated as:

$$\hat{\alpha} = \frac{n \sum_{\tau=\tau_{\min}}^{\tau_{\max}} \ln(\tau) \ln(\widehat{MSD}(\tau)) - \sum_{\tau=\tau_{\min}}^{\tau_{\max}} \ln(\tau) \sum_{\tau=\tau_{\min}}^{\tau_{\max}} \ln(\widehat{MSD}(\tau))}{n \sum_{\tau=\tau_{\min}}^{\tau_{\max}} \ln^2(\tau) - (\sum_{\tau=\tau_{\min}}^{\tau_{\max}} \ln(\tau))^2}. \quad (7)$$

In the last equation, the ensemble average MSD, $\langle \tilde{X}^2(n\Delta t) \rangle$, was replaced by the time-averaged MSD (TAMSD). The estimator of the latter for a sample $(x_1, x_2, x_3, \dots, x_N)$ measured in times $\Delta t, 2\Delta t, \dots, N\Delta t$ is defined as

$$\widehat{MSD}(n\Delta t) = \frac{1}{N-n} \sum_{k=1}^{N-n} (x_{k+n} - x_k)^2, \quad (8)$$

for $n = 0, 1, 2, \dots, N-1$.

Once $\hat{\alpha}$ is determined, the diffusion coefficient K is extracted from the intercept of the fitted regression line:

$$\hat{K} = \frac{\exp(\ln \widehat{MSD}(\tau_{\min}))}{2\tau_{\min}^{\hat{\alpha}}}. \quad (9)$$

By employing the TAMSD approach, this method ensures a more robust estimation of K in the presence of measurement noise compared to classical ensemble-averaged MSD methods. The choice of τ_{\min} and τ_{\max} is crucial, as discussed in [53], since it defines the region where noise effects are minimized while maintaining a sufficient number of data points for a reliable estimation. In our implementation, we set $\tau_{\min} = 1$ and $\tau_{\max} = 10$ to balance statistical accuracy and noise minimization. However, a more refined selection of both τ_{\min} and τ_{\max} could likely improve the robustness of the estimation. Alternatively, one could utilize non-linear regression of formula (5), with logarithm term, or its Taylor expansion, as in [53]. It could lead to a better α and K estimation results, at a cost of higher computational cost. However, the trajectories available in the challenge were usually quite short, and such an approach would often lead to higher level of statistical errors.

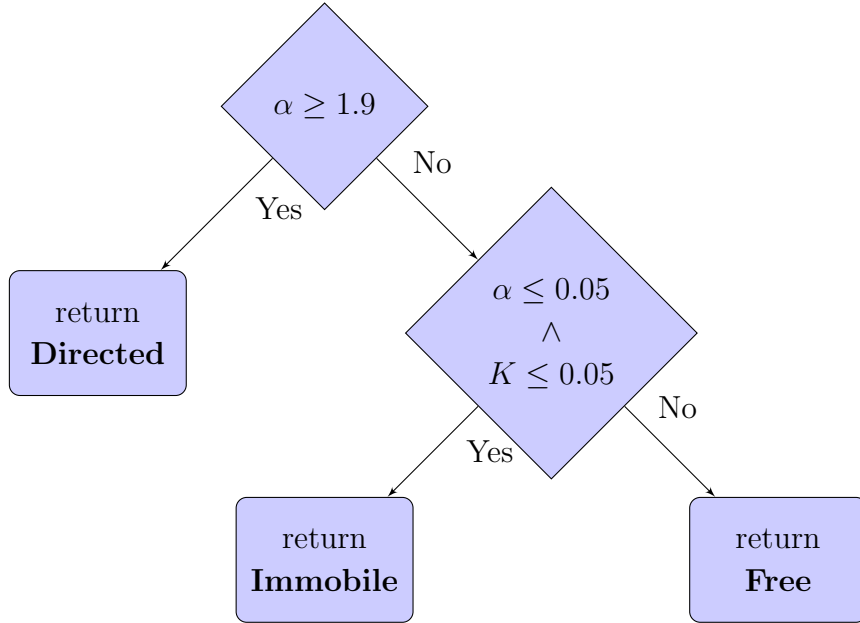


Figure 7. Our procedure for classification of segments. If for a given segment the estimated α was large, the movement of the molecule in that segment was classified as directed. If, on the other hand, both α and K were small, the molecule was considered to be immobile. In the remaining cases, the movement of the molecule was assumed to be free.

3.1.4. Classification of segments Classification of segments of the trajectories turned out to be the most challenging part of the single-trajectory task. We tested several approaches, including the one that we proposed for the 1st AnDi Challenge [52] (referred to as the GB-Classifier I) and finally ended up with a very simple procedure which classifies the segments based on the estimated values of α and K (referred to as the naive method). Moreover, we completely neglected the “confined” state in the procedure (see Ref. [46] for explanation). Taking it into account would make the method more complicated with practically no impact on its accuracy.

The naive method is shown in Fig. 7. If for a given segment the estimated α was large, the movement of the molecule in that segment was classified as directed. If, on the other hand, both α and K were small, we considered the molecule to be immobile. In the remaining cases, we considered the movement of the molecule to be free.

In Table 7 (Sec. 4.3), a brief comparison of the naive method and the GB-Classifier I is presented. A third method, being a combination of those two, is also considered there (GB-Classifier II). In the latter approach, a gradient boosting classifier working with the features from Appendix A was used to distinguish the “confinement” state from the other ones. As for the rest of the states, it was processed further with the naive method from Fig. 7.

3.1.5. Additional features from TDA The engineering of the features for the 1st AnDi Challenge (see Ref. [52] and Appendix A) was guided by physical intuition and the

statistical properties of the diffusive models under consideration. Since the models in the second challenge differ from the previous ones, we decided to further enrich the feature set by adding characteristics derived from topological data analysis (TDA) [67, 68].

Euler characteristics computed for complexes generated with the Vietoris-Rips filtration [69] combined with the order of points within the trajectory (points that occur later in trajectory, occur later in filtration) have been used as additional features for our regressor.

3.2. Ensemble task

As already mentioned in Sec. 2, the goal of the ensemble task in the 2nd AnDi Challenge was to provide statistical description of diffusive behavior of particles across an experiment [46]. A general scheme of the CINAMMON method for this task is shown in Fig. 8. Again, we decided to go for a hybrid solution.

In the first step of the procedure, a neural network is applied to identify the underlying model used to generate the trajectories. Its architecture is very similar to the one proposed for change point detection (see Fig. 4). The main difference are Max_Pooling layers [70] added after each convolution step and a Flatten layer [71]. Moreover, a softmax function was used instead of a sigmoid as the last activation function. A short comparison of the architectures is given in Table 1.

After the classification of single trajectories within the experiment, its final label was determined with a majority vote, i.e. the most frequent label across all trajectories became the overall class of the experiment. To map between the diffusive states and their parameters (α, K) , estimates of those parameters from the single-trajectory task were grouped together with the k-means algorithm [72]. No data normalization was carried out before clusterization. For the initialization of the centroids, the greedy k-means++ algorithms [73] was used. It was carried out only once for each clusterization. The number of groups was specified by the identified type of the model in most of the cases. For single-state models, only one cluster was considered. For all other models except the multi-state one, the number of clusters was set to 2. Since the multi-state model does not imply any particular number of clusters, in this case we performed the grouping sequentially for the number of clusters ranging from 2 to $2 + N$, where N is the number of (α, K) pairs. For each clustering attempt, the average silhouette score was calculated and the grouping with its highest value was selected. No specific remediation strategy was implemented for cases with low clustering performance.

Finally, the mean and standard deviations of the estimates of (α, K) in each group were calculated. The obtained values can be treated as mean and standard deviation of the parameters in the corresponding diffusive states.

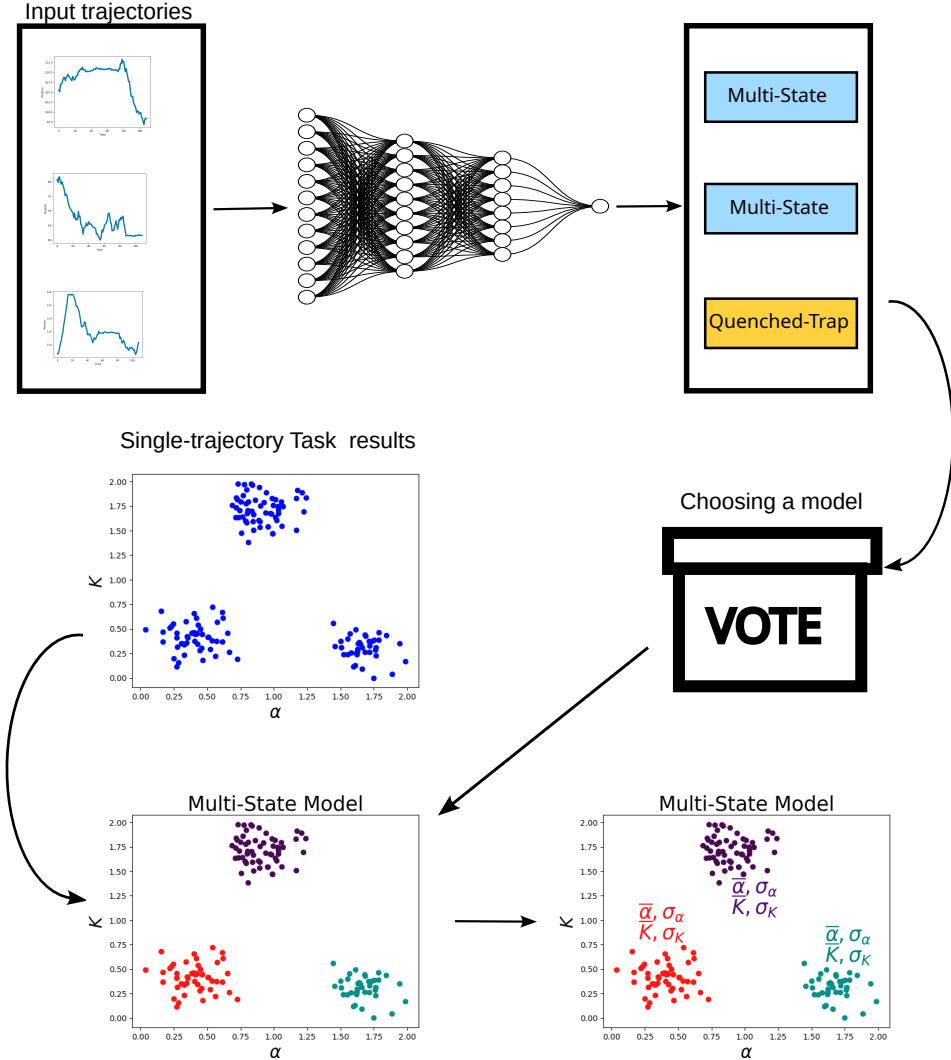


Figure 8. CINNAMON method for the ensemble task [46]. First, each trajectory is classified by a neural network and then, the diffusion model used in a given experiment is identified by majority voting. Next, the results of the single-trajectory task, i.e., the pairs (α, K) are clustered with the k -means algorithm. It is simply expected that trajectories representing the same physical model should reveal similar characteristics. If the model chosen in the first step is the multi-state model, then the number of clusters is determined based on the silhouette score. Otherwise, the model itself determines their number. In the final step, the mean and the standard deviation of the estimates of (α, K) in each group are calculated. They are treated as the mean and the standard deviation of the parameters in the corresponding diffusive states.

4. Results

Most of the results presented in this section are based on the benchmark dataset provided by the organizers of the 2nd AnDi Challenge [74]. This dataset covers a wide range of biological and physical scenarios, such as multistate diffusion, trapping, confinement, and dimerization, with experiments designed to explore diverse diffusive parameters. This allows for a thorough evaluation of algorithms for change point

Layer	Single-trajectory task	Ensemble task
DAIN	$(B, T, 2)$	$(B, 150, 2)$
Conv1D	$(B, T, 128)$	$(B, 148, 128)$
Max_Pooling1D	—	$(B, 49, 128)$
Conv1D	$(B, T, 64)$	$(B, 47, 64)$
Max_Pooling1D	—	$(B, 23, 64)$
LSTM	$(B, T, 128)$	$(B, 23, 256)$
Dropout	$(B, T, 128)$	$(B, 23, 256)$
LSTM	$(B, T, 64)$	$(B, 23, 128)$
Dropout	$(B, T, 64)$	$(B, 23, 128)$
Attention	$(B, 64)$	$(B, 128)$
Dropout	$(B, 64)$	$(B, 128)$
Flatten	—	$(B, 128)$
Dense	$(B, 128)$	$(B, 128)$
Dropout	$(B, 128)$	$(B, 128)$
Dense	$(B, 64)$	$(B, 64)$
Dropout	$(B, 64)$	$(B, 64)$
Dense	$(B, 1)$	$(B, 5)$

Table 1. Comparison of the neural network architectures used in the single-trajectory (see Fig. 4) and the ensemble tasks. The biggest difference between the architectures are the Max_Pooling layers added after every convolution step in the ensemble task, as well as the additional Flatten layer. The shapes of the layers differ as well. Another difference, not shown in the table, is the last activation function – in the ensemble task a softmax function was used instead of a sigmoid. B is the size of each data batch ($B = 32$ was used throughout this work), T is the length of the trajectory.

detection, classification, and characterization. The results of the final round of the AnDi Challenge 2 are presented in Tables 2-3. Our team (called HSC AI) placed 13th in the single-trajectory task and 7th in the ensemble task.

4.1. Change point detection

The training and validation loss and accuracy values are presented in Figure 10 and Figure 9, respectively. Four neural network classifier architectures were compared: the full model described in Sec. 3.1.1, as well as three simplified variants (CNN+LSTM, CNN-only, and LSTM-only). All architectures incorporate the DAIN layer for preprocessing. The early plateau in the CNN-only model demonstrates that adding LSTM components significantly improves model performance, as the CNN+LSTM and the full models continue to decrease their loss throughout the 10 epochs. This confirms our hypothesis that capturing temporal dependencies is crucial for this task. Regarding the attention mechanism, while its contribution appears modest in the loss curves, accuracy metrics show that the full model achieves slightly better performance than

Global rank	Team	RMSE (CP)	JSC (CP)	MAE (alpha)	MSLE (K)	F1 (diff. type)	RMSE rank	JSC rank	MAE rank	MSLE rank	F1 rank	MRR
1	UCL SAM	1.639	0.703	0.175	0.015	0.968	1	1	1	1	1	1.000
2	SPT-HIT	1.693	0.650	0.217	0.022	0.915	3	13	8	2	2	0.358
3	HNU	1.658	0.482	0.178	0.060	0.871	2	10	2	10	10	0.260
4	M3	1.738	0.649	0.184	0.024	0.652	5	4	3	4	15	0.220
5	bjyong	1.896	0.664	0.211	0.252	0.879	7	2	6	11	9	0.202
6	SU-FIONA	2.426	0.579	0.194	0.024	0.885	10	6	4	3	7	0.199
7	Unfriendly AI	1.709	0.632	0.241	0.042	0.903	4	5	9	8	4	0.187
8	KCL	1.803	0.533	0.214	0.030	0.882	6	8	7	6	8	0.145
9	EmetBrown	4.439	0.084	0.309	0.056	0.910	17	17	12	9	3	0.129
10	BIOMED-UCA	2.138	0.570	0.275	0.026	0.859	9	7	10	5	12	0.127
11	Nanoinjas	3.677	0.246	0.203	1.870	0.899	12	12	5	16	5	0.126
12	KNU-ON	2.659	0.488	0.307	0.031	0.756	11	9	11	7	14	0.101
13	HSC AI	4.025	0.193	0.393	1.402	0.896	15	15	15	15	6	0.087
14	Alntgommawork	1.994	0.447	0.563	0.298	0.545	8	11	17	13	16	0.083
15	ICSO UPV	4.056	0.211	0.380	5.255	0.861	16	13	14	17	11	0.072
16	D.AnDi	3.879	0.204	0.472	0.275	0.354	14	14	16	12	17	0.070
17	DeepSPT	4.894	0.186	0.336	0.424	0.822	18	16	13	14	13	0.069
18	far naz	3.829	0.023	1.476	94.564	0.293	13	18	18	18	18	0.060

Table 2. Final results of the 2nd AnDi Challenge - single-trajectory task. Our team (HSC AI) is placed 13th. See Ref. [46] for the explanation of all measures used in the table.

Global rank	Team	W1 (alpha)	W1 (K)	alpha rank	k rank	MRR
1	UCL SAM	0.138	0.058	1	4	0.250
2	DeepSPT	0.267	0.050	9	1	0.222
3	Nanoninjas	0.192	0.051	3	2	0.167
4	bjyong	0.188	0.084	2	7	0.129
5	SPT-HIT	0.231	0.057	6	3	0.100
6	ICSO UPV	0.218	0.067	4	5	0.090
7	HSC AI	0.230	0.256	5	8	0.065
8	Unfriendly AI	0.238	0.072	7	6	0.062
9	EmetBrown	0.259	0.622	8	11	0.043
10	BIOMED-UCA	0.275	0.534	10	9	0.042
11	KCL	0.448	0.593	11	10	0.038

Table 3. Final results of the 2nd AnDi Challenge - ensemble task. Our team (HSC AI) is placed 7th. See Ref. [46] for the explanation of all measures used in the table.

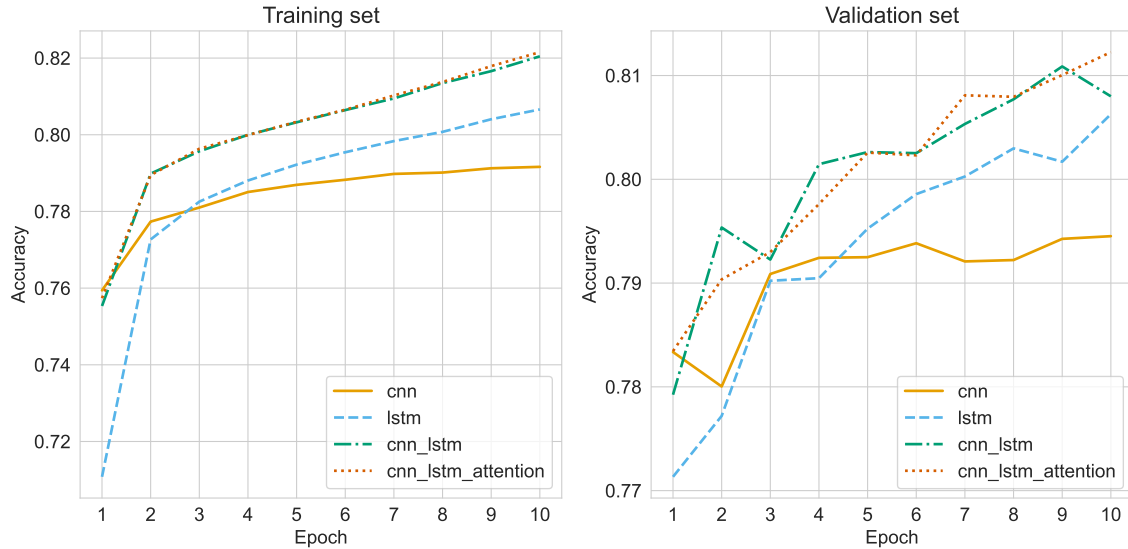


Figure 9. Training and validation accuracy for different variants of the neural network classifier. The full model, described in Sec. 3.1.1, is compared with three simplified versions (CNN+LSTM, CNN-only, and LSTM-only).

CNN+LSTM (0.8140 accuracy vs. 0.8087). Even such a small improvement can be considered as valuable in the context of change-point detection. Additionally, the attention module adds minimal computational overhead to the model (194 640 vs. 190 415 parameters).

The results of the single-trajectory task for the benchmark dataset are presented in Table 4. With the exception of experiments 6 and 8, where this metric is equal to 0, root-mean-square error (RMSE) is at a similar level in all experiments. A greater variety of results is seen for the Jaccard similarity coefficient (JSC). No clear relationship

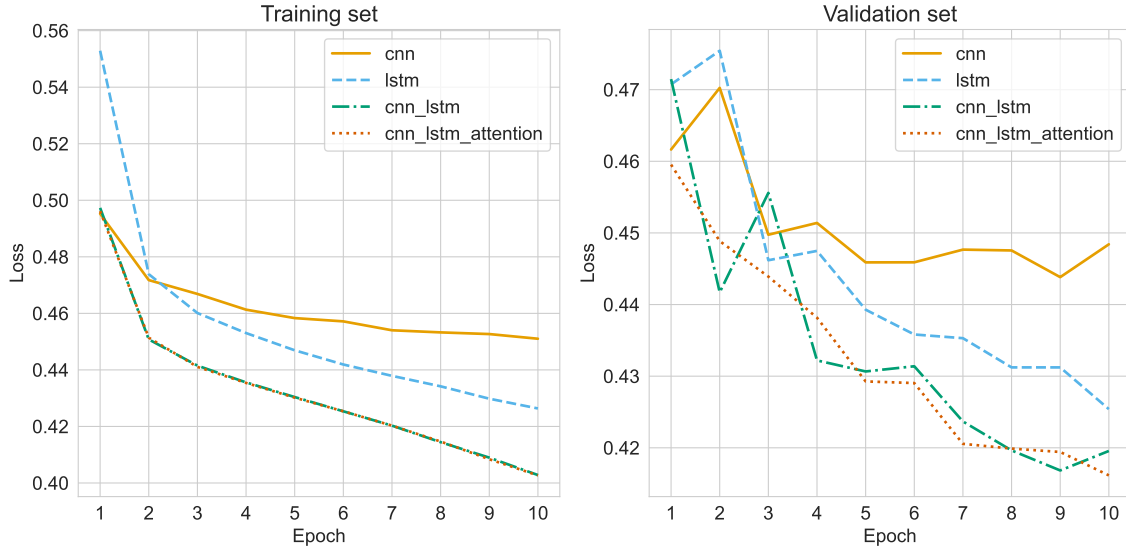


Figure 10. Training and validation loss for different variants of the neural network classifier. The full model, described in Sec. 3.1.1, is compared with three simplified versions (CNN+LSTM, CNN-only, and LSTM-only).

is apparent between the model of the experiment and the effectiveness of change point detection.

Exp	num_trajs	RMSE (CP)	JSC (CP)	MSLE (K)	MAE (alpha)	F1 (diff. type)
1	1280	4.512061	0.012563	2.585260	0.567237	0.979381
2	8983	4.737913	0.074069	0.540352	0.814740	0.997437
3	1348	3.655631	0.384653	2.435835	0.328328	0.852941
4	1192	4.524786	0.257439	2.581110	0.372193	0.601671
5	6485	4.582201	0.155559	0.561066	0.378303	0.993404
6	1172	0.000000	0.452656	3.122132	0.507152	0.973729
7	1222	4.962651	0.058971	2.621429	0.471954	0.979050
8	1524	0.000000	0.958172	4.888330	0.483815	0.951444
9	1857	4.602225	0.136440	1.082408	1.052998	0.213957

Table 4. Results in the single-trajectory task for the benchmark dataset. No clear relationship is apparent between the model of the experiment and the effectiveness of change point detection.

4.2. Parameters estimation

The results of the estimation of parameter α using the features of the first AnDi challenge are presented in Fig. 11. They were obtained for trajectories of length 100. The original feature set was created to solve the problem of distinguishing between different types of anomalous diffusion. In case of regression of α , only some of them turned out to

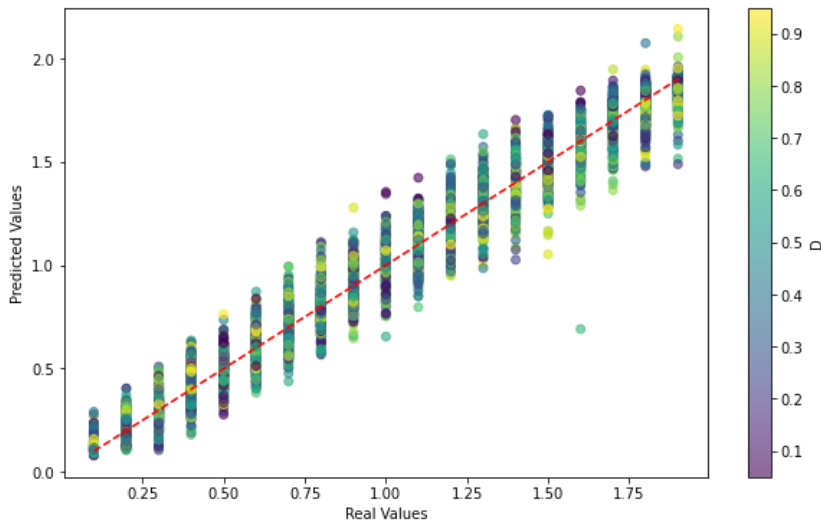


Figure 11. Prediction of α with the gradient boosting regressor and the feature set from the 1st AnDi Challenge. The error metrics for these estimates are presented in Table 5.

be useful. The significance of the most important ones is shown in the Fig. 12. The influence of the other features on the estimations is negligible. The most important features (sorted by significance) are as follows:

- anomalous exponent estimation based on fitting the empirical TAMSD,
- statistics based on p -variation (for $p = 2, 3$),
- mean maximal excursion,
- empirical velocity autocorrelation functions.

For details regarding the features, please refer to Appendix A.

The results for the generalized diffusion coefficient K are presented in Fig. 13. We see that for both α and K , the accuracy of the prediction decreases with the increasing values of the parameters. It is worth to mention that we tried to improve the estimation of K by making use of the gradient boosting regressor we have already used for α . However, the predictions were practically the same. Although quite surprising at first glance, this outcome can be easily explained. The feature set presented in Appendix A contains already the estimator of K described in Sec. 3.1.3. And, after building the regressor for K it turned out that this estimator is the only important feature. The remaining ones can be neglected. This is the reason why we observed practically no difference between the methods. It also indicate that the feature set may be not appropriate for the problem at hand.

Adding topological descriptors to the set of characteristics did not improve the results either. Their effect on the estimation was negligible. There are a few potential reasons for that outcome. First of all, since all of the diffusion models were based on the fractional Brownian motion, they might not generate trajectories with significant, persistent topological differences that the Euler characteristic can effectively distinguish.

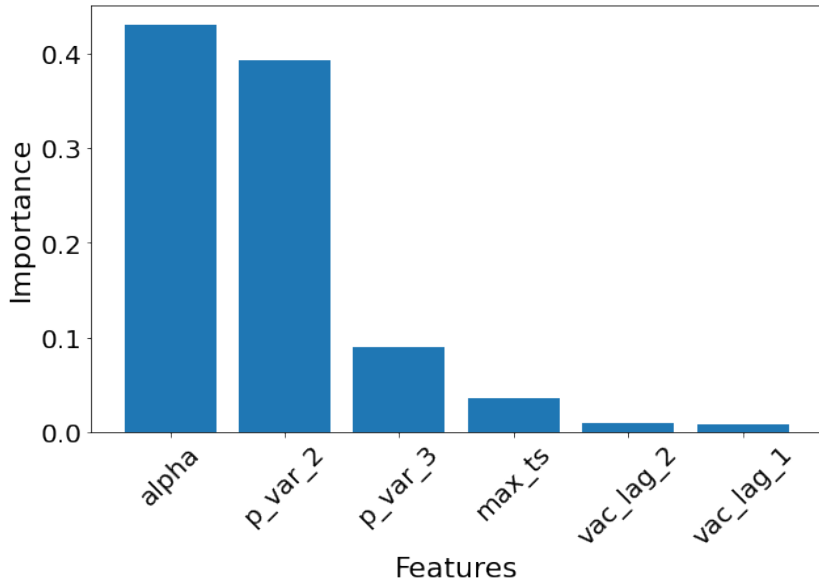


Figure 12. Importance of the six most important features for estimating α using gradient boosting. `alpha` is the standard estimation of the anomalous exponent, based on fitting the empirical TAMSD to the model (A.1). `p_var_2` and `p_var_3` correspond to exponents γ^p fitted to the empirical p -variation (Eq. A.17) with $p = 2$ and $p = 3$, respectively. `max_ts` is the mean maximal excursion (Eq. (A.9)). And finally, `vac_lag_2` and `vac_lag_1` are the velocity autocorrelation functions at lags 2 and 1 (Eq. (A.5)). Impact of the remaining features on estimation is minimal. The importances reflect how often the features are used to split the data across all trees.

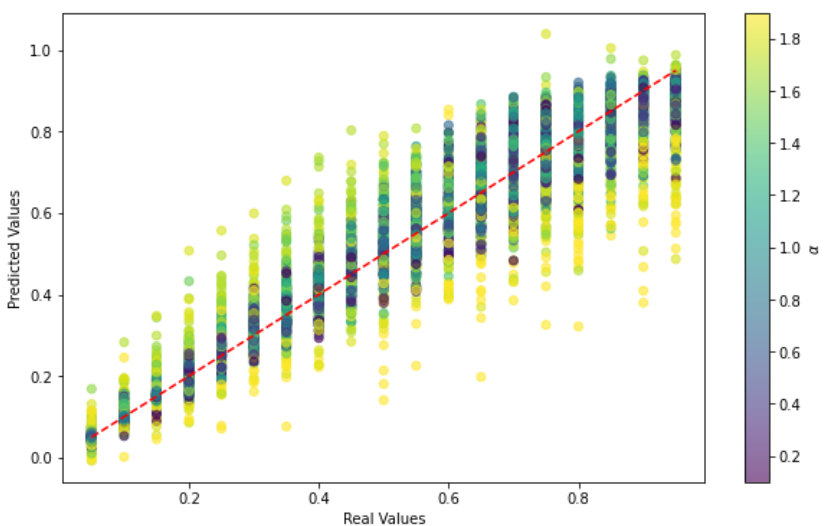


Figure 13. Prediction of K with the method from Sec. 3.1.3. The error metrics for these estimates are presented in Table 6.

Secondly, the filtration we have chosen causes the initial parts of the trajectory to have a greater impact on the topological descriptor values than the final parts. As there is no reason to favor the initial points of the trajectory, this phenomenon may have had a negative impact on the quality of the proposed descriptor. More details regarding the performance of different approaches can be seen in Tables 5-6.

	R2	MSE	MAE
AnDi 1 features	0.973	0.008	0.069
TDA + AnDi 1 features	0.973	0.008	0.069

Table 5. Estimation results for the anomalous exponent α . Two variants of the regressors are compared. The one was trained only with the features described in Appendix A (refered to as AnDi 1 features). In case of the other, the feature set was extended with the characteristics from TDA (see Sec. 3.1.5).

	R2	MSE	MAE
Estimator	0.864	0.010	0.062
AnDi 1 features	0.923	0.006	0.051
TDA + AnDi 1 features	0.923	0.006	0.051

Table 6. Estimation results for the generalized diffusion coefficient K . The analytical method from Sec. 3.1.3 is compared with two variants of the regressors. The one was trained with the features described in Appendix A (refered to as AnDi 1 features). In case of the other, the feature set was extended with the characteristics from TDA (see Sec. 3.1.5).

4.3. Diffusive states

Despite of the simplicity of our method we obtained high F_1 -score on the benchmark dataset (Table 4). For most of the experiments, the index was higher than 0.95. Worse results were obtained for the Immobile Traps experiments (number 3 and 9) and the Confinement experiment (number 4). In these cases, the F_1 -score was 0.85, 0.21 and 0.60, respectively. Worse results in case of Confinement model based experiment was expected, because our method does not take the confinement state into account (see Sec. 3.1.4)

One can of course ask the question how the predictive power of our method will change after taking that state into consideration. A comparison of our naive method with two simple feature-based classifiers is presented in Table 7. We see that the naive method indeed outperforms the classifiers, which may indicate that the feature set designed for the previous edition of the AnDi Challenge may require far-reaching adjustments for the new type of data.

	Naive	GB-Classifier I	GB-Classifier II
AVG	0.838	0.812	0.808
Weighted AVG	0.906	0.835	0.837

Table 7. F-1 score values for the classification of diffusive states, averaged over all experiments. Weighted averages are given in the second row (weights are the number of trajectories in each experiment). The definition of the classification methods is given in Sec. 3.1.4. The “naive” one was used through this paper.

4.4. Ensemble Task

The outcomes for each benchmark experiment are shown in Table 8. It should be emphasized here that these results are grounded in parameter estimates for α and K derived from the single-trajectory task. The dependency of the ensemble task on the prior one is particularly noticeable in the estimation of the α parameter, with the best results for this parameter achieved in experiments 2, 3, and 4. The relationship between the results of the two tasks is more intricate for parameter K . In experiments 2 and 4, the K parameter results are moderately successful for the single-trajectory task but substantially poor for the ensemble task, whereas Experiment 5 yields good results for both tasks.

Exp	W1 (K)	W1 (alpha)
1	0.915170	0.531545
2	0.819725	0.782572
3	0.502521	0.247958
4	0.063257	0.146702
5	0.376822	0.190814
6	0.291466	0.304549
7	0.754769	0.289931
8	0.486562	0.395450
9	1.158701	0.722865

Table 8. Results for benchmark experiments in the ensemble task. W1 stands for the Wasserstein distance (please refer to Ref. [46] for further details).

Our method of recognizing the experiment model failed. Only one experiment from the benchmark was correctly classified (Table 9). There is a clear bias in the prediction towards the single-state model. In many cases, misclassification of the model led to poor selection of the number of states.

To test how much impact these misclassifications had on the final results of our method, we replaced the predicted physical models with the real ones. The results are shown in Table 10. As can be seen, this change did not significantly improve the results. Only in the case of experiment 3, a noticeable improvement is visible.

	Real	Predicted
Exp. 1	Multi-state	Confinement
Exp. 2	Dimerization	Dimerization
Exp. 3	Immobile traps	Single State
Exp. 4	Confinement	Dimerization
Exp. 5	Dimerization	Single State
Exp. 6	Dimerization	Single State
Exp. 7	Multi-state	Single State
Exp. 8	Multi-state	Single State
Exp. 9	Immobile traps	Dimerization

Table 9. Results for classification of physical models in the benchmark dataset.

Exp	W1 (K)	W1 (alpha)
1	0.929019	0.531413
2	0.819689	0.782573
3	0.339198	0.164255
4	0.063257	0.146702
5	0.259741	0.159874
6	0.339915	0.341425
7	0.736490	0.283159
8	0.554527	0.398018
9	1.159196	0.722828

Table 10. Results for benchmark experiments in the ensemble task when the information regarding real physical models is used. For all but the experiment 3, this additional information did not significantly improve the results.

5. Conclusions

In this paper, a hybrid method for change point detection and parameter estimation for anomalous diffusion has been presented. The method is a mixture of deep-learning algorithms, feature-based regression and analytical estimation. Having a good experience with feature-based methods from the 1st AnDi Challenge, we tried to use methods with a relatively high level of interpretability, at least as parts of the procedure, also in the just-completed second edition of the competition.

This time, however, the effectiveness of our approach lagged significantly behind the best solutions based on neural networks. We placed 13th in the single-trajectory task and 7th in the ensemble one. From the results it follows that the estimation of the generalized diffusion coefficient K was the weakest point of our approach. Since we used for that purpose an analytical method considered one of the best in its category, this result demonstrates how much of an advantage deep learning methods now have over the analytical approach. Changing the estimation method of K to a gradient-boosted

regressor did not help, indicating that the feature set we used may require far-reaching adjustments for the new type of data.

Acknowledgements

Jakub Malinowski acknowledges the support of the Dioscuri program initiated by the Max Planck Society, jointly managed with the National Science Centre (Poland), and mutually funded by the Polish Ministry of Science and Higher Education and the German Federal Ministry of Education and Research.

Data availability statement

No new data sets were created or analyzed in this study.

Appendix A. Feature set for gradient boosting regression

As already mentioned in Sec. 3.1.2, we used a method based on gradient boosting to estimate the diffusion exponent α . The set of features constructed for the first AnDi challenge and then further optimized was used to characterize the trajectories. A detailed description of all features can be found in Refs. [30, 34, 52].

Both the original feature set for the 1st AnDi challenge and its extension are listed in Table A1. Here, we briefly describe them for the convenience of a reader.

Original features	Additional features
Anomalous exponent	D'Agostino-Pearson test statistic
Diffusion coefficient	Kolmogorov-Smirnov statistic against χ^2 distribution
Asymmetry	Noah exponent
Efficiency	Moses exponent
Empirical velocity autocorrelation function	Joseph exponent
Fractal dimension	Detrending moving average
Maximal excursion	Average moving window characteristics
Mean maximal excursion	Maximum standard deviation
Mean gaussianity	
Mean-squared displacement ratio	
Kurtosis	
Statistics based on p -variation	
Straightness	
Trappedness	

Table A1. The features used to characterize the SPT trajectories. The original set of features for the 1st AnDi Challenge have been extended afterwards to improve the performance of the classifier [52].

Anomalous exponent In our set of features, we included 4 estimates for the anomalous exponent α , calculated using the following methods:

- the standard estimation, based on fitting the empirical time-averaged MSD (TAMSD) from Eq. (8) to the model MSD for anomalous diffusion,

$$\widehat{MSD}(n\Delta t) \sim K_\alpha t^\alpha, \quad (\text{A.1})$$

- 3 estimation methods proposed for the trajectories with noise [53], under the assumption that the noise is normally distributed with zero mean:

- using estimator

$$\hat{\alpha} = \frac{n_{max} \sum_{n=1}^{n_{max}} \ln(n) \ln(\widehat{MSD}(n\Delta t)) - \sum_{n=1}^{n_{max}} \ln(n) \left(\sum_{n=1}^{n_{max}} \ln(\widehat{MSD}(n\Delta t)) \right)}{n_{max} \sum_{n=1}^{n_{max}} \ln^2(n) - (\sum_{n=1}^{n_{max}} \ln(n))^2},$$

with n_{max} equal to 0.1 times the trajectory length, rounded to nearest lower integer (but not less than 4),

- simultaneous fitting of parameters \hat{K} , $\hat{\alpha}$ and $\hat{\sigma}$ in the equation

$$\widehat{MSD}(n\Delta t) = 2d\hat{K}(n\Delta t)^{\hat{\alpha}} + \hat{\sigma}^2,$$

where d denotes dimension, K is the generalized diffusion coefficient and σ^2 - the variance of noise,

- simultaneous fitting of parameters \hat{D} and $\hat{\alpha}$ in the equation

$$\widehat{MSD}(n\Delta t) = 2d\hat{D}(\Delta t)^{\hat{\alpha}}(n^{\hat{\alpha}} - 1).$$

Diffusion coefficient We used the diffusion coefficient extracted from the fit of the empirical TA-MSD (Eq. (8)) to Eq. (A.1).

Asymmetry The asymmetry of a trajectory can be derived from the gyration tensor [16]. For a 2D random walk of N steps, the tensor is given by

$$\mathbf{T} = \begin{pmatrix} \frac{1}{N} \sum_{j=1}^N (x_j - \langle x \rangle)^2 & \frac{1}{N} \sum_{j=1}^N (x_j - \langle x \rangle)(y_j - \langle y \rangle) \\ \frac{1}{N} \sum_{j=1}^N (x_j - \langle x \rangle)(y_j - \langle y \rangle) & \frac{1}{N} \sum_{j=1}^N (y_j - \langle y \rangle)^2 \end{pmatrix}, \quad (\text{A.2})$$

where $\langle x \rangle = (1/N) \sum_{j=1}^N x_j$ is the average of x coordinates over all steps in the random walk. The asymmetry is defined as

$$A = -\log \left(1 - \frac{(\lambda_1 - \lambda_2)^2}{2(\lambda_1 + \lambda_2)^2} \right), \quad (\text{A.3})$$

where λ_1 and λ_2 are the principle radii of gyration, i.e., the eigenvalues of the tensor \mathbf{T} [75]. Higher values of A indicate a greater tendency for a preferred direction.

Efficiency Efficiency E relates the net squared displacement of a particle to the sum of squared step lengths,

$$E = \frac{|X_{N-1} - X_0|^2}{(N-1) \sum_{i=1}^{N-1} |X_i - X_{i-1}|^2}. \quad (\text{A.4})$$

Empirical velocity autocorrelation function Empirical velocity autocorrelation function [76] for lag 1 and point n is defined as:

$$\chi_n = \frac{1}{N-1} \sum_{i=0}^{N-2} (X_{i+1+n} - X_{i+n})(X_{i+1} - X_i) \quad (\text{A.5})$$

In our model, we used χ_n for points $n = 1$ and $n = 2$.

Fractal dimension Fractal dimension is a measure of the space-filling capacity of a pattern (a trajectory in our case). According to Katz and George [77], the fractal dimension of a planar curve may be calculated as

$$D_f = \frac{\ln N}{\ln(NdL^{-1})}, \quad (\text{A.6})$$

where L is the total length of the trajectory, N is the number of steps, and d is the largest distance between any two positions.

Maximal excursion Maximal excursion of the particle is given by the formula:

$$ME = \frac{\max_i (X_{i+1} - X_i)}{|X_{N-1} - X_0|}. \quad (\text{A.7})$$

Mean maximal excursion Given the largest distance traveled by a particle,

$$D_N = \max_i |X_i - X_0|, \quad (\text{A.8})$$

the mean maximal excursion is defined as its standardized value, i.e.:

$$T_n = \frac{\max_i (|X_i - X_0|)}{\sqrt{\hat{\sigma}_N^2(t_N - t_0)}}. \quad (\text{A.9})$$

Here, $\hat{\sigma}_N$ is a consistent estimator of the standard deviation of D_N ,

$$\hat{\sigma}_N^2 = \frac{1}{2N\delta t} \sum_{j=1}^N \|X_j - X_{j-1}\|_2^2. \quad (\text{A.10})$$

Mean gaussianity Gaussianity $g(n)$ [78] checks the Gaussian statistics of increments of a trajectory and is defined as

$$g(n) = \frac{2 \langle r_n^4 \rangle}{3 \langle r_n^2 \rangle^2}, \quad (\text{A.11})$$

where $\langle r_n^k \rangle$ denotes the k th moment of the trajectory at time lag n :

$$\langle r_n^k \rangle = \frac{1}{N-n} \sum_{i=1}^{N-n} |X_{i+n} - X_i|^k. \quad (\text{A.12})$$

Instead of looking at Gaussianities at single time lags, we will include the mean over all lags as one of the features:

$$\langle g \rangle = \frac{1}{N} \sum_{i=1}^N g(n). \quad (\text{A.13})$$

Mean-squared displacement ratio MSD ratio gives information about the shape of the corresponding MSD curve. We will define it as

$$MSDR(n_1, n_2) = \frac{\langle r_{n_1}^2 \rangle}{\langle r_{n_2}^2 \rangle} - \frac{n_1}{n_2}, \quad (\text{A.14})$$

where $n_1 < n_2$. We simply took $n_2 = n_1 + \Delta t$ and calculate an averaged ratio for every trajectory.

Kurtosis To calculate kurtosis [75], the position vectors X_i are projected onto the dominant eigenvector \vec{r} of the gyration tensor (A.2),

$$x_i^p = X_i \cdot \vec{r}. \quad (\text{A.15})$$

Kurtosis is then defined as the fourth moment of x_i^p ,

$$Kur = \frac{1}{N} \sum_{i=1}^N \frac{(x_i^p - \bar{x}^p)^4}{\sigma_{x^p}^4}, \quad (\text{A.16})$$

with \bar{x}^p being the mean projected position and σ_{x^p} - the standard deviation of x^p .

Statistics based on p -variation The empirical p -variation is given by the formula [79,80]:

$$V_m^{(p)} = \sum_{i=0}^{\frac{N}{m}-1} |X_{(i+1)m} - X_{im}|^p. \quad (\text{A.17})$$

We defined 6 features based on $V_m^{(p)}$:

- power γ^p fitted to p -variation for lags 1 to 5 [79],
- statistics P used in Ref. [34], based on the monotonicity changes of $V_m^{(p)}$ as a function of m :

$$P = \begin{cases} 0 & \text{if } V_m^{(p)} \text{ does not change the monotonicity,} \\ 1 & \text{if } V_m^{(p)} \text{ is convex for the highest } p \text{ for which it is not monotonous,} \\ -1 & \text{if } V_m^{(p)} \text{ is concave for the highest } p \text{ for which it is not monotonous.} \end{cases}$$

Straightness Straightness S measures the average direction change between subsequent steps. It relates the net displacement of a particle to the sum of all step lengths,

$$S = \frac{|X_{N-1} - X_0|}{\sum_{i=1}^{N-1} |X_i - X_{i-1}|}. \quad (\text{A.18})$$

The closer it is to 1, the straighter the trajectory is. In contrast, S close to 0 indicates no preferred direction on the trajectory.

Trappedness With trappedness we will refer to the probability that a diffusing particle is trapped in a bounded region with radius r_0 . A comparison of analytical and Monte Carlo results for confined diffusion allowed Saxton [16] to estimate this probability with

$$P(K, t, r_0) = 1 - \exp \left(0.2048 - 0.25117 \left(\frac{Kt}{r_0^2} \right) \right). \quad (\text{A.19})$$

Here, r_0 is approximated by half of the maximum distance between any two positions along a given trajectory. K in Eq. (A.19) is estimated by fitting the first two points of the MSD curve (i.e. it is the so called short-time diffusion coefficient).

D'Agostino-Pearson test statistic D'Agostino-Pearson κ^2 test statistic [81, 82] is a goodness-of-fit measure that aims to establish whether or not a given sample comes from a normally distributed sample. It is defined as

$$\kappa^2 = Z_1(g_1) + Z_2(K), \quad (\text{A.20})$$

where K is the sample kurtosis given by Eq. (A.16) and $g_1 = m_3/m_2^{3/2}$ is the sample skewness with m_j being the j th sample central moment. The transformations Z_1 and Z_2 should bring the distributions of the skewness and kurtosis as close to the standard normal as possible. Their definitions may be found elsewhere [81, 82].

Kolmogorov-Smirnov statistic against χ^2 distribution The Kolmogorov-Smirnov statistic quantifies the distance between the empirical distribution function of the sample $F_n(X)$ and the cumulative distribution function $G_n(X)$ of a reference distribution,

$$D_n = \sup_X |F_n(X) - G_n(X)|. \quad (\text{A.21})$$

Here, n is the number of observations (i.e. the length of a trajectory). The value of this statistic for the empirical distribution of squared increments of a trajectory against the sampled χ^2 distribution has been taken as the next feature. The rationale of such choice is that for a Gaussian trajectory the theoretical distribution of squared increments is the mentioned χ^2 distribution.

Noah, Moses, and Joseph exponents For processes with stationary increments, there are in principle two mechanisms that violate the Gaussian central limit theorem and produce anomalous scaling of MSD [83]: long-time increment correlations or a flat-tailed increment distribution (in the latter case the second moment is divergent). An anomalous scaling can also be induced by a non-stationary increment distribution. In this case, we deal with the Moses effect.

All three effects may be quantified by exponents, which will be used as features in our extended set of attributes. Given a stochastic process X_t and the corresponding increment process $\delta_t(\tau) = X_{t+\tau} - X_t$, the Joseph, Moses and Noah exponents are defined as follows.

(i) Joseph exponent J is estimated from the ensemble average of the rescaled range statistic:

$$E \left[\frac{\max_{1 \leq s \leq t} [X_s - \frac{s}{t} X_t] - \min_{1 \leq s \leq t} [X_s - \frac{s}{t} X_t]}{\sigma_t} \right] \sim t^J,$$

$$E \left[\frac{R_t}{S_t} \right] \sim t^J,$$

where R_t is calculated as $R_t = \max_{1 \leq s \leq t} [X_s - \frac{s}{t} X_t] - \min_{1 \leq s \leq t} [X_s - \frac{s}{t} X_t]$ and S_t is standard deviation of process X_t , and E is the mathematical expectation.

(ii) Moses exponent M is determined from the scaling of the ensemble probability distribution of the sum of the absolute value of increments, which can be estimated by the scaling of the median of the probability distribution of $Y_t = \sum_{s=0}^{t-1} |\delta_s|$:

$$m[Y_t] \sim t^{M-\frac{1}{2}}$$

(iii) Noah exponent L is extracted from the scaling of the ensemble probability distribution of the sum of increment squares, which can be estimated by the scaling of the median of the probability distribution of $Z_t = \sum_{s=0}^{t-1} \delta_s^2$:

$$m[Z_t] \sim t^{2L+2M-1}$$

Detrending moving average The detrending moving average (DMA) statistic is given by

$$DMA(\tau) = \frac{1}{N - \tau + 1} \sum_{i=\tau}^N (X_i - \bar{X}_i^\tau)^2, \quad (\text{A.22})$$

for $\tau = 1, 2, \dots$, where \bar{X}_i^τ is a moving average of τ observations, i.e. $\bar{X}_i^\tau = \frac{1}{\tau+1} \sum_{j=0}^\tau X_{i-j}$ [84, 85]. In our model, we used two values of DMA for each trajectory as input features, namely $DMA(1)$ and $DMA(2)$.

Average moving window characteristics We added eight features based on the formula

$$MW = \frac{1}{2(N+1)} \sum_{i=0}^N \left| \operatorname{sgn} \left(\bar{X}_{i+1}^{(m)} - \bar{X}_i^{(m)} \right) - \operatorname{sgn} \left(\bar{X}_{i+1}^{(m)} - \bar{X}_i^{(m)} \right) \right|, \quad (\text{A.23})$$

where $\overline{X}^{(m)}$ denotes a statistic of the process calculated within the window of length m and sgn is the signum function. In particular, we used the mean and the standard deviation for \overline{X} and calculated MW with windows of lengths $m = 10$ and $m = 20$ separately for x and y coordinates.

Maximum standard deviation The idea of the moving window helped us to introduce another two features based on the standard deviation σ_m of the process calculated within a window of length m . They are given by

$$MXM = \frac{\max(\sigma_m(t))}{\min(\sigma_m(t))} \quad (\text{A.24})$$

and

$$MXC = \frac{\max |\sigma_m(t+1) - \sigma_m(t)|}{\sigma}, \quad (\text{A.25})$$

where σ denotes the overall standard deviation of the sample. We used the window of length $m = 3$ and calculated the features for both coordinates separately.

- [1] Hao Shen, Lawrence J. Tauzin, Rashad Baiyasi, Wenxiao Wang, Nicholas Moringo, Bo Shuang, and Christy F. Landes. Single particle tracking: From theory to biophysical applications. *Chemical Reviews*, 117:7331–7376, 2017.
- [2] Jean Perrin. Mouvement brownien et molécules. *J. Phys. Theor. Appl.*, 9(1):5–39, 1910.
- [3] Ivar Nordlund. A new determination of Avogadro’s number from Brownian motion of small mercury spherules. *Z. Phys. Chem.*, 87:40, 1914.
- [4] Carlo Manzo and Maria F Garcia-Parajo. A review of progress in single particle tracking: from methods to biophysical insights. *Reports on Progress in Physics*, 78(12):124601, 2015.
- [5] Kenichi Suzuki, Ken Ritchie, Eriko Kajikawa, Takahiro Fujiwara, and Akihiro Kusumi. Rapid hop diffusion of a G-protein-coupled receptor in the plasma membrane as revealed by single-molecule techniques. *Biophysical Journal*, 88(5):22–22, apr 2005.
- [6] Mathias P Clausen and B Christoffer Lagerholm. Visualization of plasma membrane compartmentalization by high-speed quantum dot tracking. *Nano Letters*, 13(6):2332–2337, Jun 2013.
- [7] Steffen J Sahl, Marcel Leutenegger, Michael Hilbert, Stefan W Hell, and Christian Eggeling. Fast molecular tracking maps nanoscale dynamics of plasma membrane lipids. *Proceedings of the National Academy of Sciences of the United States of America*, 107(15):6829–6834, Apr 2010.
- [8] Christopher W Cairo, Rossen Mirchev, and David E Golan. Cytoskeletal regulation couples Ifa-1 conformational changes to receptor lateral mobility and clustering. *Immunity*, 25(2):297–308, Aug 2006.
- [9] Daniel Lingwood and Kai Simons. Lipid rafts as a membrane-organizing principle. *Science*, 327(5961):46–50, jan 2010.
- [10] Christian Eggeling, Christian Ringemann, Rebecca Medda, Günter Schwarzmann, Konrad Sandhoff, Svetlana Polyakova, Vladimir N Belov, Birk Hein, Claas von Middendorff, Andreas Schönle, and Stefan W Hell. Direct observation of the nanoscale dynamics of membrane lipids in a living cell. *Nature*, 457(7233):1159–1162, Feb 2009.
- [11] Akihiro Kusumi, Chieko Nakada, Ken Ritchie, Kotono Murase, Kenichi Suzuki, Hideji Murakoshi, Rinshi S Kasai, Junko Kondo, and Takahiro Fujiwara. Paradigm shift of the plasma membrane concept from the two-dimensional continuum fluid to the partitioned fluid: high-speed single-molecule tracking of membrane molecules. *Annual Review of Biophysics and Biomolecular Structure*, 34:351–378, 2005.

- [12] Pietro Massignan, Carlo Manzo, Juan A. Torreno-Pina, Maria F. García-Parajo, Maciej Lewenstein, and Gerald J. Lapeyre Jr. Nonergodic subdiffusion from Brownian motion in an inhomogeneous medium. *Physical Review Letters*, 112:150603, Apr 2014.
- [13] Hong Qian, Michael P. Sheetz, and Elliot L. Elson. Single particle tracking. Analysis of diffusion and flow in two-dimensional systems. *Biophysical Journal*, 60:910–921, 1991.
- [14] Ralf Metzler, Jae-Hyung Jeon, Andrey G. Cherstvy, and Eli Barkai. Anomalous diffusion models and their properties: non-stationarity, non-ergodicity, and ageing at the centenary of single particle tracking. *Physical Chemistry Chemical Physics*, 16:24128–24164, 2014.
- [15] Rainer Klages, Günter Radons, and Igor M Sokolov. *Anomalous transport*. Wiley Online Library, 2008.
- [16] Michael J Saxton. Lateral diffusion in an archipelago. Single-particle diffusion. *Biophysical Journal*, 64:1766–80, 1993.
- [17] Denis S. Grebenkov, Mahsa Vahabi, Elena Bertseva, László Forró, and Sylvia Jeney. Hydrodynamic and subdiffusive motion of tracers in a viscoelastic medium. *Physical Review E*, 88:040701, Oct 2013.
- [18] Andrzej Fuliński. Fractional Brownian motions: memory, diffusion velocity, and correlation functions. *Journal of Physics A: Mathematical and Theoretical*, 50:054002, 2017.
- [19] Carina Raupach, Daniel Paranhos Zitterbart, Claudia T. Mierke, Claus Metzner, Frank A. Müller, and Ben Fabry. Stress fluctuations and motion of cytoskeletal-bound markers. *Physical Review E*, 76:011918, Jul 2007.
- [20] Stanislav Burov, S. M. Ali Tabei, Toan Huynh, Michael P. Murrell, Louis H. Philipson, Stuart A. Rice, Margaret L. Gardel, Norbert F. Scherer, and Aaron R. Dinner. Distribution of directional change as a signature of complex dynamics. *Proceedings of the National Academy of Sciences*, 110(49):19689–19694, 2013.
- [21] Vincent Tejedor, Olivier Bénichou, Raphael Voituriez, Ralf Jungmann, Friedrich Simmel, Christine Selhuber-Unkel, Lene B. Oddershede, and Ralf Metzler. Quantitative analysis of single particle trajectories: Mean maximal excursion method. *Biophysical Journal*, 98(7):1364–1372, 2010.
- [22] Krzysztof Burnecki, Eldad Kepten, Yuval Garini, Grzegorz Sikora, and Aleksander Weron. Estimating the anomalous diffusion exponent for single particle tracking data with measurement errors - an alternative approach. *Scientific Reports*, 5:11306, 2015.
- [23] Alex Krizhevsky, Ilya Sutskever, and Geoffrey E Hinton. Imagenet classification with deep convolutional neural networks. *Communications of the ACM*, 60(6):84–90, 2017.
- [24] Geoffrey Hinton, Li Deng, Dong Yu, George E Dahl, Abdel-rahman Mohamed, Navdeep Jaitly, Andrew Senior, Vincent Vanhoucke, Patrick Nguyen, Tara N Sainath, et al. Deep neural networks for acoustic modeling in speech recognition: The shared views of four research groups. *IEEE Signal Processing Magazine*, 29(6):82–97, 2012.
- [25] Ashish Vaswani, Noam Shazeer, Niki Parmar, Jakob Uszkoreit, Llion Jones, Aidan N Gomez, Łukasz Kaiser, and Illia Polosukhin. Attention is all you need. *Advances in Neural Information Processing Systems*, 30:5998–6008, 2017.
- [26] Nilah Monnier, Syuan-Ming Guo, Masashi Mori, Jun He, Péter Lénárt, and Mark Bathe. Bayesian approach to MSD-based analysis of particle motion in live cells. *Biophysical Journal*, 103:616–626, 2012.
- [27] Samudrajit Thapa, Michael A. Lomholt, Jens Krog, Andrey G. Cherstvy, and Ralf Metzler. Bayesian analysis of single-particle tracking data using the nested-sampling algorithm: maximum-likelihood model selection applied to stochastic-diffusivity data. *Physical Chemistry Chemical Physics*, 20(46):29018–29037, 2018.
- [28] Lijian Chen, Kevin E. Bassler, Joseph L. McCauley, and Gemunu H. Gunaratne. Anomalous scaling of stochastic processes and the Moses effect. *Physical Review E*, 95:042141, Apr 2017.
- [29] Thorsten Wagner, Alexandra Kroll, Chandrashekara R. Haramagatti, Hans-Gerd Lipinski, and Martin Wiemann. Classification and segmentation of nanoparticle diffusion trajectories in cellular micro environments. *PLoS ONE*, 12(1):e0170165, 2017.

- [30] Patrycja Kowalek, Hanna Loch-Olszewska, and Janusz Szwabiński. Classification of diffusion modes in single-particle tracking data: Feature-based versus deep-learning approach. *Physical Review E*, 100:032410, Sep 2019.
- [31] Gorka Muñoz-Gil, Miguel Angel García-March, Carlo Manzo, José D Martín-Guerrero, and Maciej Lewenstein. Single trajectory characterization via machine learning. *New Journal of Physics*, 22(1):013010, jan 2020.
- [32] Gorka Muñoz-Gil, Giovanni Volpe, Miguel Angel García-March, Ralf Metzler, Maciej Lewenstein, and Carlo Manzo. The anomalous diffusion challenge: single trajectory characterisation as a competition. *Emerging Topics in Artificial Intelligence 2020*, Aug 2020.
- [33] Joanna Janczura, Patrycja Kowalek, Hanna Loch-Olszewska, Janusz Szwabiński, and Aleksander Weron. Classification of particle trajectories in living cells: Machine learning versus statistical testing hypothesis for fractional anomalous diffusion. *Physical Review E*, 102:032402, Sep 2020.
- [34] Hanna Loch-Olszewska and Janusz Szwabiński. Impact of feature choice on machine learning classification of fractional anomalous diffusion. *Entropy*, 22(12), 2020.
- [35] Patrice Dosset, Patrice Rassam, Laurent Fernandez, Cedric Espenel, Eric Rubinstein, Emmanuel Margeat, and Pierre-Emmanuel Milhiet. Automatic detection of diffusion modes within biological membranes using backpropagation neural network. *BMC Bioinformatics*, 17:197, 2016.
- [36] Stefano Bo, Falko Schmidt, Ralf Eichhorn, and Giovanni Volpe. Measurement of anomalous diffusion using recurrent neural networks. *Physical Review E*, 100:010102, Jul 2019.
- [37] Naor Granik, Lucien E. Weiss, Elias Nehme, Maayan Levin, Michael Chein, Eran Perlson, Yael Roichman, and Yoav Shechtman. Single-particle diffusion characterization by deep learning. *Biophysical Journal*, 117(2):185–192, Jul 2019.
- [38] Alessia Gentili and Giorgio Volpe. Characterization of anomalous diffusion classical statistics powered by deep learning (CONDOR). *Journal of Physics A: Mathematical and Theoretical*, 54(31):314003, jul 2021.
- [39] Miłosz Gajowczyk and Janusz Szwabiński. Detection of anomalous diffusion with deep residual networks. *Entropy*, 23(6), 2021.
- [40] Gorka Muñoz-Gil, Giovanni Volpe, Miguel Angel García-March, Erez Aghion, Aykut Argun, Chang Beom Hong, Tom Bland, Stefano Bo, J. Alberto Conejero, Nicolás Firbas, Óscar Garibo i Orts, Alessia Gentili, Zihan Huang, Jae-Hyung Jeon, Hélène Kabbech, Yeongjin Kim, Patrycja Kowalek, Diego Krapf, Hanna Loch-Olszewska, Michael A. Lomholt, Jean-Baptiste Masson, Philipp G. Meyer, Seongyu Park, Borja Requena, Ihor Smal, Taeyeun Song, Janusz Szwabiński, Samudrajit Thapa, Hippolyte Verdier, Giorgio Volpe, Artur Widera, Maciej Lewenstein, Ralf Metzler, and Carlo Manzo. Objective comparison of methods to decode anomalous diffusion. *Nature Communications*, 12(1), oct 2021.
- [41] Michael J. Saxton and Ken Jacobson. Single-particle tracking: Applications to membrane dynamics. *Annual Review of Biophysics and Biomolecular Structure*, 26(1):373–399, 1997. PMID: 9241424.
- [42] Marc Taraban, Hongli Zhan, Andrew E Whitten, David B Langley, Kathleen S Matthews, Liskin Swint-Kruse, and Jill Trewhella. Ligand-induced conformational changes and conformational dynamics in the solution structure of the lactose repressor protein. *Journal of Molecular Biology*, 376(2):466–481, 2008.
- [43] Hans Frauenfelder, Stephen G. Sligar, and Peter G. Wolynes. The energy landscapes and motions of proteins. *Science*, 254(5037):1598–1603, 1991.
- [44] Michael J. Saxton. Single-particle tracking: models of directed transport. *Biophys. J.*, 67(5):2110–2119, Nov 1994.
- [45] Daniel Lingwood and Kai Simons. Lipid rafts as a membrane-organizing principle. *Science*, 327(5961):46–50, 2010.
- [46] Gorka Muñoz-Gil, Harshith Bachimanchi, Jesus Pineda, Benjamin Midtvedt, Maciej Lewenstein, Ralf Metzler, Diego Krapf, Giovanni Volpe, and Carlo Manzo. Quantitative evaluation of

methods to analyze motion changes in single-particle experiments [Registered Report Stage 1 Protocol]. *Nature Communications*, 12 2023.

[47] Borja Requena, Sergi Maso-Orriols, Joan Bertran, Maciej Lewenstein, Carlo Manzo, and Gorka Munoz-Gil. Inferring pointwise diffusion properties of single trajectories with deep learning. *Biophysical Journal*, 122:4360, 2023.

[48] Xiang Qu, Yi Hu, Wenjie Cai, Yang Xu, Hu Ke, Guolong Zhu, and Zihan Huang. Semantic segmentation of anomalous diffusion using deep convolutional networks. *Physical Review Research*, 6:013054, 2024.

[49] Joanna Janczura, Michał Balcerek, Krzysztof Burnecki, Adal Sabri, Matthias Weiss, and Diego Krapf. Identifying heterogeneous diffusion states in the cytoplasm by a hidden Markov model. *New Journal of Physics*, 23(5):053018, May 2021.

[50] Daniel Han, Nickolay Korabel, Runze Chen, Mark Johnston, Anna Gavrilova, Victoria J Allan, Sergei Fedotov, and Thomas A Waigh. Deciphering anomalous heterogeneous intracellular transport with neural networks. *eLife*, 9:52224, 2020.

[51] Ian Goodfellow, Yoshua Bengio, and Aaron Courville. *Deep Learning*. MIT Press, 2016. <http://www.deeplearningbook.org>.

[52] Patrycja Kowalek, Hanna Loch-Olszewska, Łukasz Łaszczuk, Jarosław Opała, and Janusz Szwabiński. Boosting the performance of anomalous diffusion classifiers with the proper choice of features. *Journal of Physics A: Mathematical and Theoretical*, 55(24):244005, May 2022.

[53] Yann Lanoiselée, Grzegorz Sikora, Aleksandra Grzesiek, Denis S. Grebenkov, and Agnieszka Wyłomańska. Optimal parameters for anomalous-diffusion-exponent estimation from noisy data. *Physical Review E*, 98:062139, Dec 2018.

[54] Benoit B. Mandelbrot and John W. Van Ness. Fractional Brownian motions, fractional noises and applications. *SIAM Review*, 10(4):422–437, 1968.

[55] Jakub Malinowski. CINNAMON: Code and data for the ANDI Challenge 2024 (WUST). https://github.com/Malinon/andi_challenge_2_wust, 2024.

[56] Jie Li, Paul Fearnhead, Piotr Fryzlewicz, and Tengyao Wang. Automatic change-point detection in time series via deep learning. *Journal of the Royal Statistical Society Series B: Statistical Methodology*, 86(2):273–285, 01 2024.

[57] Nikolaos Passalis, Anastasios Tefas, Juho Kannainen, Moncef Gabbouj, and Alexandros Iosifidis. Deep adaptive input normalization for time series forecasting. *IEEE Transactions on Neural Networks and Learning Systems*, 31(9):3760–3765, 2020.

[58] Serkan Kiranyaz, Onur Avci, Osama Abdeljaber, Turker Ince, Moncef Gabbouj, and Daniel J. Inman. 1D convolutional neural networks and applications: A survey. *Mechanical Systems and Signal Processing*, 151:107398, 2021.

[59] Sepp Hochreiter and Jürgen Schmidhuber. Long short-term memory. *Neural Computation*, 9:1735–80, 12 1997.

[60] Gang Liu and Jiabao Guo. Bidirectional lstm with attention mechanism and convolutional layer for text classification. *Neurocomputing*, 337:325–338, 2019.

[61] Nitish Srivastava, Geoffrey Hinton, Alex Krizhevsky, Ilya Sutskever, and Ruslan Salakhutdinov. Dropout: A simple way to prevent neural networks from overfitting. *Journal of Machine Learning Research*, 15(56):1929–1958, 2014.

[62] Xavier Glorot and Yoshua Bengio. Understanding the difficulty of training deep feedforward neural networks. In *Proceedings of the thirteenth international conference on artificial intelligence and statistics*, pages 249–256. JMLR Workshop and Conference Proceedings, 2010.

[63] Diederik P Kingma and Jimmy Ba. Adam: A method for stochastic optimization. *arXiv preprint arXiv:1412.6980*, 2014.

[64] Tianqi Chen and Carlos Guestrin. XGBoost: A scalable tree boosting system. KDD '16, page 785–794, New York, NY, USA, 2016. Association for Computing Machinery.

[65] Yan-Yan Song and LU Ying. Decision tree methods: applications for classification and prediction. *Shanghai Archives of Psychiatry*, 27(2):130, 2015.

- [66] Jerome H. Friedman. Greedy function approximation: A gradient boosting machine. *The Annals of Statistics*, 29(5):1189–1232, 2001.
- [67] Robert Ghrist. Barcodes: the persistent topology of data. *Bulletin of the American Mathematical Society*, 45:61–76, 2007.
- [68] G. Carlsson. Topology and data. *Bulletin of the American Mathematical Society*, 46:255–308, 2009.
- [69] Paweł Dłotko and Davide Gurnari. Euler characteristic curves and profiles: a stable shape invariant for big data problems. *GigaScience*, 12:giad094, 11 2023.
- [70] Afia Zafar, Muhammad Aamir, Nazri Mohd Nawi, Ali Arshad, Saman Riaz, Abdulrahman Alruban, Ashit Kumar Dutta, and Sultan Almotairi. A comparison of pooling methods for convolutional neural networks. *Applied Sciences*, 12(17):8643, 2022.
- [71] Ernest Jeczmionek and Piotr A Kowalski. Flattening layer pruning in convolutional neural networks. *Symmetry*, 13(7):1147, 2021.
- [72] James MacQueen. Some methods for classification and analysis of multivariate observations. In *Proceedings of the Fifth Berkeley Symposium on Mathematical Statistics and Probability, Volume 1: Statistics*, volume 5, pages 281–298. University of California Press, 1967.
- [73] Christoph Grunau, Ahmet Alper Özüdoğru, Václav Rozhoň, and Jakub Tětek. *A Nearly Tight Analysis of Greedy k-means++*, pages 1012–1070. Proceedings of the 2023 Annual ACM-SIAM Symposium on Discrete Algorithms (SODA), 2023.
- [74] Gorka Muñoz-Gil, Harshith Bachimanchi, Jesus Pineda, Benjamin Midtvedt, Borja Requena, Gabriel Fernández Fernández, Maciej Lewenstein, Ralf Metzler, Diego Krapf, Giovanni Volpe, and Carlo Manzo. Andi 2 benchmark dataset, December 2024.
- [75] Jo A. Helmuth, Christoph J. Burckhardt, Petros Koumoutsakos, Urs F. Greber, and Ivo F. Sbalzarini. A novel supervised trajectory segmentation algorithm identifies distinct types of human adenovirus motion in host cells. *Journal of Structural Biology*, 159:347–358, 2007.
- [76] Stephanie C. Weber, Andrew J. Spakowitz, and Julie A. Theriot. Bacterial chromosomal loci move subdiffusively through a viscoelastic cytoplasm. *Phys. Rev. Lett.*, 104:238102, Jun 2010.
- [77] Michael J. Katz and Edwin B. George. Fractals and the analysis of growth paths. *Bulletin of Mathematical Biology*, 47(2):273–286, Mar 1985.
- [78] Dominique Ernst, Jürgen Köhler, and Matthias Weiss. Probing the type of anomalous diffusion with single-particle tracking. *Physical Chemistry Chemical Physics*, 16:7686–7691, 2014.
- [79] Krzysztof Burnecki and Aleksander Weron. Fractional Lévy stable motion can model subdiffusive dynamics. *Physical Review E*, 82:021130, 2010.
- [80] Marcin Magdziarz, Aleksander Weron, Krzysztof Burnecki, and Joseph Klafter. Fractional Brownian motion versus the continuous-time random walk: A simple test for subdiffusive dynamics. *Physical Review Letters*, 103:180602, 2009.
- [81] Ralph B. D'Agostino. An omnibus test of normality for moderate and large size samples. *Biometrika*, 58(2):341–348, 1971.
- [82] Ralph D'Agostino and E. S. Pearson. Tests for departure from normality. empirical results for the distributions of b_2 and $\sqrt{b_1}$. *Biometrika*, 60(3):613–622, 1973.
- [83] Erez Aghion, Philipp G Meyer, Vidushi Adlakha, Holger Kantz, and Kevin E Bassler. Moses, Noah and Joseph effects in Lévy walks. *New Journal of Physics*, 23(2):023002, feb 2021.
- [84] Grzegorz Sikora. Statistical test for fractional Brownian motion based on detrending moving average algorithm. *Chaos, Solitons & Fractals*, 116:54–62, 2018.
- [85] Michał Balcerak, Krzysztof Burnecki, Grzegorz Sikora, and Agnieszka Wyłomańska. Discriminating Gaussian processes via quadratic form statistics. *Chaos: An Interdisciplinary Journal of Nonlinear Science*, 31(6):063101, 2021.